ASME Journal of Applied Mechanics
Online journal at:
https://asmedigitalcollection.asme.org/appliedmechanics

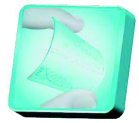

Ultra-Broadband Sound Reduction in Nonlocal Ventilating Structures With Double Mode Degeneracy

Yonghui Zhang
Key Laboratory of Dynamics and Control of Flight Vehicle of Ministry of Education, School of Aerospace Engineering, Beijing Institute of Technology, Beijing 100081, China
e-mail: yh_zhang@bit.edu.cn

Lei Zhang
Institute of Large Structures for Advanced Industrial Equipment, Beijing Institute of Technology, Zhuhai 519088, China
e-mail: lei_zh@bit.edu.cn

Xiaoming Zhou[1]
Key Laboratory of Dynamics and Control of Flight Vehicle of Ministry of Education, School of Aerospace Engineering, Beijing Institute of Technology, Beijing 100081, China
e-mail: zhxming@bit.edu.cn

Channel-type structures based on Fano resonances show significant potential in simultaneous control of sound isolation and air ventilation. Broad isolation bandwidth is a crucial factor to the Fano-based model but usually relying on multiple element arrangement. In this work, a novel mechanism based on the nonlocal effect via direct mode couplings is proposed to broaden the isolation bandwidth of ventilating structures. The studied model is a ternary structure consisting of two coiling channels coupled to a straight orifice. Two Fano-based transmission valleys, which are independently controlled by two coiling channels, can be merged by designing single-mode degeneracy. Without introducing more elements, the nonlocal mode coupling, achieved by the direct hole connection between channels, is found to produce the double-mode degeneracy behavior such that three transmission valleys can be combined to obtain an ultra-broadband sound insulation. A coupled-mode model is developed to derive the mode degeneracy condition of Fano resonances, and illustrate the working mechanism to manipulate double-mode degeneracy. Both numerical and experimental analyses are conducted to demonstrate the superior performance of the nonlocal effect for a significant increase of isolation bandwidth in Fano-based open sound barriers. [DOI: 10.1115/1.4070148]

Keywords: sound isolation, air ventilation, nonlocal effect, coupled-mode theory, Fano resonance, direct mode coupling, mode degeneracy, mechanical properties of materials, structures, wave propagation

1 Introduction

Ventilating sound insulation structures have great application potential in various engineering scenarios. Acoustic ventilating barriers can be categorized according to the arrangement of controlling elements, placed externally or internally with respect to the air-guiding system. The side-branch structure arranged externally allows the perfect air flow, and is important for designing acoustic liners to damp engine noise. Different configurations, mostly based on the resonant effect, have been proposed [1–13]. On the other hand, there are some circumstances where structures need to be embedded within the air-flowing system like silencing windows or walls. The helical channel coiled around a straight orifice can serve as an effective model utilizing the Fano interference to block sounds while enabling air ventilation [14–23]. The Fano resonance originates from the interference between discrete and continuous states, which are supported by coiling and straight channels, respectively, and can produce asymmetric transmission dips. A transmission valley can be formed between adjacent transmission dips, leading to high-efficiency sound insulation in a finite bandwidth [24–26].

Soundproofing bandwidths of Fano-based ventilating structures can be enhanced in lateral-coupled or longitudinal-coupled cell structures [27], where there is a trade-off between the geometric size, air ventilation, and sound isolation. Other broadband mechanisms have also been proposed, including the synergy of the consecutive Fano resonances and monopole-dipole mode superposition [28], as well as the critical mode coupling that can lead to near-zero sound transmission in a finite band rather than at isolated frequencies [20]. Recent studies also highlight the importance of the nonlocal effect in achieving broadband sound isolation under ventilation conditions. In the binary structure where the helical channel is blocked at the rear, the nonlocal effect via direct couplings between straight and coiling parts is found playing a central role in broadening the isolation bandwidth [29]. As another configuration, a microperforated panel is introduced between straight and coiling channels, providing a strong damping coupling between them. The resonance-induced high transmission outside of the transmission valley can be suppressed by damping, leading to the broadband sound reduction [30].

In this work, the nonlocal effect via direct mode couplings would be further exploited to develop a different mechanism to broaden the isolation bandwidth in Fano-based ventilating structures. We focus on the model where two coiling channels are coupled to a straight one. Each coiling channel supports independently tuned Fano-based transmission valleys. Two transmission valleys can be merged under single-mode degeneracy of Fano resonances.

[1]Corresponding author.
Manuscript received June 18, 2025; final manuscript received September 29, 2025; published online October 31, 2025. Assoc. Editor: Guoliang Huang.

Without adding more elements, we show that the direct mode coupling, physically realized by the hole connection, can lead to the double-mode degeneracy behavior such that three transmission valleys can be combined, giving rise to an ultra-broadband sound insulation. Numerical modeling shows that the octave bandwidth has nearly tripled after the direct coupling is added, revealing the superior capability of the nonlocal effect for a significant increase of the isolation bandwidth. Experimental studies will be conducted to demonstrate the broadband behavior of open sound barriers.

2 Theoretical Modeling

2.1 Geometric Model. Consider a plane acoustic wave of angular frequency ω propagating in a rectangular waveguide of the width w_0 and height h_0, and two different coiling channels and a straight one are embedded within the waveguide, as sketched in Fig. 1(*a*). Three channels are arranged in a parallel manner, having the width w_j, height h_j and length L_j for the jth ($j = 1, 2, 3$) channel. Consider the plane-wave mode in each region of the system. Acoustic wave interaction with the channeling structure can be characterized by an analytic model as shown in Fig. 1(*b*), where channels can be homogenized into continuum media of cross-sectional area $S_j = w_1 h_j$ and equal length $L = L_1$ with effective acoustic velocity $c_j = c_0 L/L_j$ and effective impedance $Z_j = w_1/w_j Z_0$. Notice that $\rho_0 = 1.21\ \mathrm{kg/m^3}$ and $c_0 = 343\ \mathrm{m/s}$ are air density and sound velocity, and $Z_0 = \rho_0 c_0$ and $S_0 = w_0 h_0$ are defined.

Based on the analytic model, the time-harmonic ($e^{i\omega t}$) pressure and particle velocity (along the x direction) fields in the jth region ($j = 1, 2, 3$) of the system can be expressed as

$$\begin{cases} p_j(x) & = A_j^+ e^{-ik_j x} + A_j^- e^{ik_j x} \\ v_j(x) & = \frac{A_j^+}{Z_j} e^{-ik_j x} - \frac{A_j^-}{Z_j} e^{ik_j x} \end{cases} \tag{1}$$

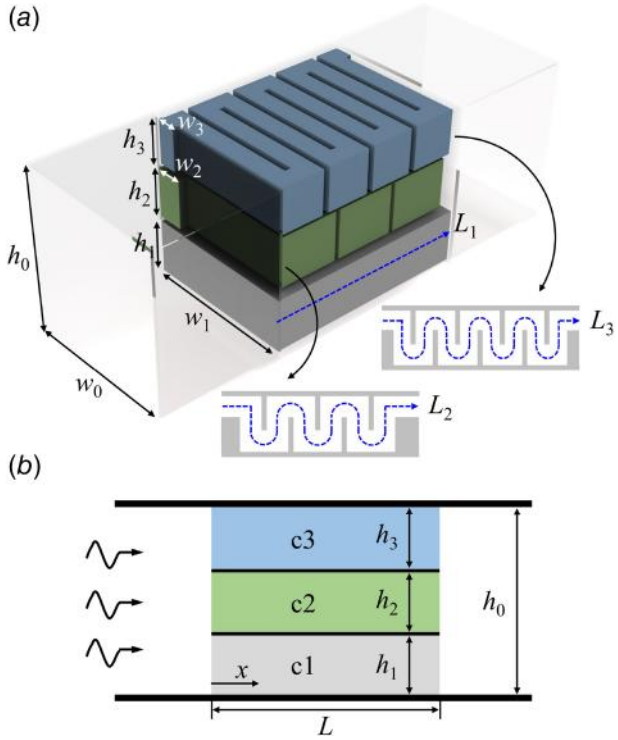

Fig. 1 (*a*) Schematic diagram of three-channel structures for broadband sound isolation and air ventilation where two coiling channels coupled to a straight one. (*b*) Effective acoustic model of three-channel structures where coiling channels are equivalent to straight ones with effective acoustic parameters.

where $k_j = \omega/c_j$. A_j^+ and A_j^- denote the complex amplitudes of rightward and leftward traveling waves, respectively. At interfaces $x = 0$ and $x = L$, the pressure is continuous and the volume flow is conservative, giving rise to

$$\begin{cases} p_j(0) = 1 + R, & Z_0 \sum_{j=1}^{3} S_j v_j(0) = S_0(1 - R) \\ p_j(L) = T, & Z_0 \sum_{j=1}^{3} S_j v_j(L) = S_0 T \end{cases} \tag{2}$$

where R and T are acoustic reflection and transmission coefficients.

Single-coiling channels support the Fabry–Pérot resonance, and the mth-order resonant frequencies of the channels c2 and c3 are given, respectively, by

$$f_{c2}^m = \frac{mc_0}{2L_2}, \quad f_{c3}^m = \frac{mc_0}{2L_3}, \quad m = 1, 2, \ldots \tag{3}$$

The resonant state is of monopole (dipole) mode when m is an odd (even) number. Zero transmission can be achieved when two states are of different mode types and have degenerate resonant frequencies [31]. As an example, Figs. 2(*a*) and 2(*b*) show acoustic energy transmission of two different coiling channels calculated by Eq. (2) for system parameters $L = 100\ \mathrm{mm}$, $L_2 = 388\ \mathrm{mm}$, $L_3 = 583\ \mathrm{mm}$, $w_0 = 80\ \mathrm{mm}$, $w_1 = 76\ \mathrm{mm}$, $w_2 = 13\ \mathrm{mm}$, $w_3 = 21\ \mathrm{mm}$, $h_0 = 40\ \mathrm{mm}$, $h_1 = 7\ \mathrm{mm}$, $h_2 = 15\ \mathrm{mm}$, and $h_3 = 14\ \mathrm{mm}$. Numerical simulations based on the model of Fig. 1(*b*) are also performed by using COMSOL MULTIPHYSICS to validate theoretical results. Notice that the structural systems in Figs. 2(*a*) and 2(*b*) have been designed such that the resonant frequencies f_{c2}^2 and f_{c3}^3 are same, equal to 882 Hz. But their wave modes are of different types, exhibiting the dipole and monopole resonance as evidenced by the pressure field distribution shown in the insets. Therefore, when two channels are coupled, acoustic transmission can be greatly lowered in the nearby region of 882 Hz due to the mode degeneracy effect as displayed in Fig. 2(*c*).

Now, let the coiling channel (c2 or c3) coupled with the straight orifice (c1) that functions for air ventilation. The Fano resonance can be formed, leading to the transmission valley ranging from the odd-order to even-order frequencies of Fabry–Pérot resonances. Three low-T regions can be observed in the frequency range of interest as marked by c2-1st, c3-1st, and c3-2nd in Figs. 2(*d*) and 2(*e*). When two coiling channels are coupled to the straight one, the c2-1st and c3-2nd low-T regions can be potentially combined to broaden the sound reduction bandwidth due to the mode degeneracy at $f_{c2}^2 = f_{c3}^3$. However, it is seen that the originally degenerate modes at 882 Hz become separated in the presence of the straight pipe, shifting to 885 Hz and 877 Hz for the channel c2 and c3, respectively. Due to this frequency deviation, acoustic transmission cannot be well reduced near 882 Hz as illustrated in Fig. 2(*f*). Deep analyses regarding the mode coupling of Fano resonances are needed to understand the low-transmission mechanism. In the next section, theoretical analyses will be conducted based on the coupled-mode model to derive the low-transmission condition due to the mode degeneracy of Fano resonances.

2.2 Mode Degeneracy Condition of Fano Resonances. Consider that the f_{c2}^2 resonant state of channel c2 is coupled to the f_{c3}^3 resonant state of channel c3. Modal amplitudes of two resonant states are denoted by a_{c2} and a_{c3} with $\mathbf{a} = [a_{c2}, a_{c3}]^{\mathrm{T}}$. Define $\omega_{c2} = 2\pi f_{c2}^2$ and $\omega_{c3} = 2\pi f_{c3}^3$. The radiation losses of two states are represented by γ_{c2} and γ_{c3}. According to the temporal coupled-mode theory, the three-channel system is governed by the following equation

$$\begin{cases} -i\frac{d\mathbf{a}}{dt} & = \mathbf{H}\mathbf{a} + \mathbf{K}^{\mathrm{T}}\mathbf{s}^+ \\ \mathbf{s}^- & = \mathbf{C}\mathbf{s}^+ + \mathbf{D}\mathbf{a} \end{cases} \tag{4}$$

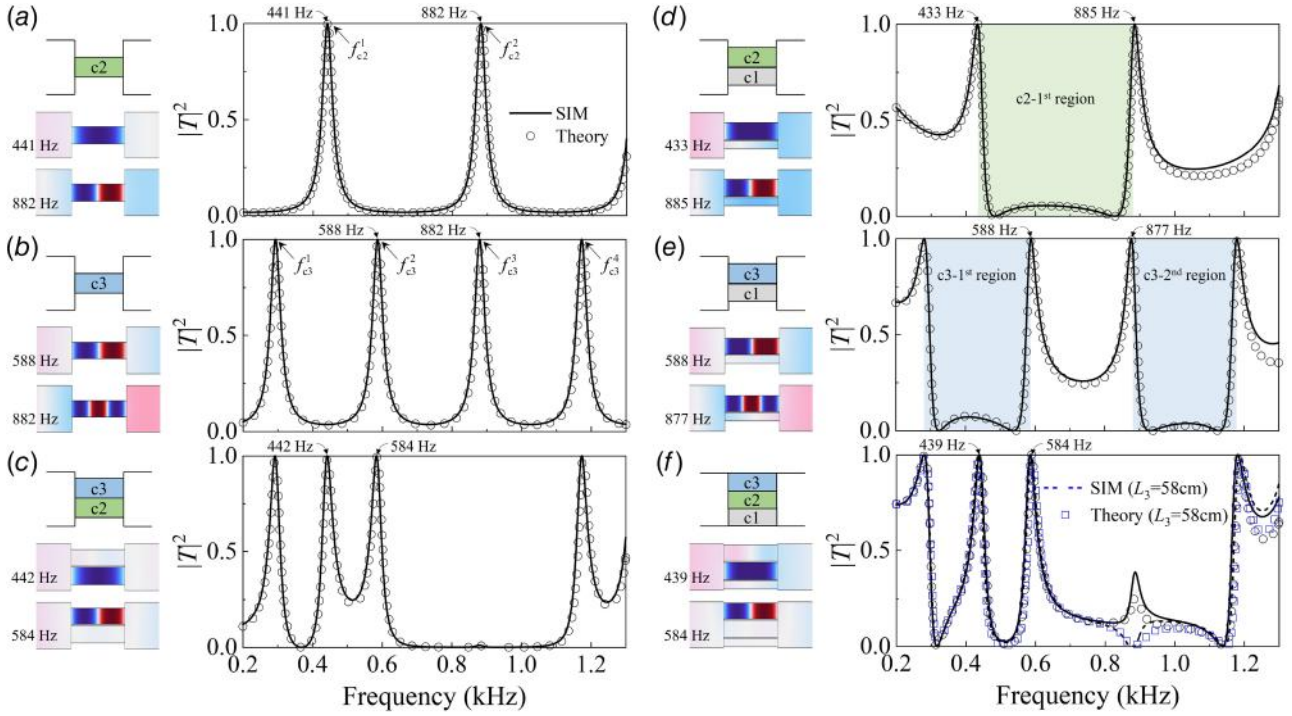

Fig. 2 Theoretical and simulation results of acoustic energy transmission for structural systems involving single channels c2 (*a*) and c3 (*b*), two coupled channels c2 and c3 (c), c1 and c2 (*d*), c1 and c3 (*e*), and three coupled channels (*f*)

with

$$\mathbf{H}=\begin{bmatrix}\omega_{c2}+i\gamma_{c2} & \kappa\\ \kappa & \omega_{c3}+i\gamma_{c3}\end{bmatrix} \tag{5}$$

$$\mathbf{C}=\begin{bmatrix}R_{c1} & T_{c1}\\ T_{c1} & R_{c1}\end{bmatrix},\ \mathbf{K}=-i\mathbf{D}=\begin{bmatrix}\sqrt{\gamma_{c2}} & \sqrt{\gamma_{c3}}\\ -\sqrt{\gamma_{c2}} & \sqrt{\gamma_{c3}}\end{bmatrix} \tag{6}$$

where κ characterizes the coupling between two resonant states. T_{c1} and R_{c1} are acoustic transmission and reflection coefficients of the system when channels c2 and c3 are rigidly blocked. Let s_L^+ and s_R^+ represent wave amplitudes of sounds impinging from the left and right sides, respectively, and s_L^- and s_R^- denote those of scattering waves traveling to the left and right. Define $\mathbf{s}^+=[s_L^+, s_R^+]^T$ and $\mathbf{s}^-=[s_L^-, s_R^-]^T$, which are related to the scattering matrix $\mathbf{S}$ by

$$\mathbf{s}^-=\mathbf{S}\,\mathbf{s}^+,\qquad \mathbf{S}=\mathbf{C}+\mathbf{D}(\omega\,\mathbf{I}-\mathbf{H})^{-1}\,\mathbf{K}^T \tag{7}$$

According to the coupled-mode model, acoustic transmission of the three-channel system can be derived as

$$T=T_{c1}-\frac{i\gamma_{c2}(R_{c1}-T_{c1})}{\omega-(\omega_{c2}+i\gamma_{c2})}+\frac{i\gamma_{c3}(R_{c1}+T_{c1})}{\omega-(\omega_{c3}+i\gamma_{c3})} \tag{8}$$

When the straight channel c1 is blocked, we have $T_{c1}=0$ and $R_{c1}=1$, and Eq. (8) is simplified as

$$T_{c23}=\frac{-i\gamma_{c2}}{\omega-(\omega_{c2}+i\gamma_{c2})}+\frac{i\gamma_{c3}}{\omega-(\omega_{c3}+i\gamma_{c3})} \tag{9}$$

Based on Eq. (9), zero transmission $T_{c23}=0$ can be obtained at the degenerate frequency $\omega=\omega_{c2}=\omega_{c3}$ as is the case in Fig. 2(*c*). At this frequency, acoustic transmission of the three-channel structure reads $T=T_{c1}$, which explains the enhanced transmission near 882 Hz in Fig. 2(*f*).

To derive the theoretical condition for zero transmission $|T|=0$ of the three-channel system, the matrix $\mathbf{C}$ in Eq. (6) is written equivalently as

$$\mathbf{C}=e^{i\phi}\begin{bmatrix}r_{c1} & it_{c1}\\ it_{c1} & r_{c1}\end{bmatrix} \tag{10}$$

where r_{c1} and ϕ are the amplitude and phase of R_{c1}, respectively, and $it_{c1}=T_{c1}e^{-i\phi}$. Notice that r_{c1} and t_{c1} are both real values. According to Eq. (8), acoustic transmission T is rewritten as

$$T=\frac{it_{c1}(\Delta\omega_3\Delta\omega_2+\gamma_{c3}\gamma_{c2})+ir_{c1}(\gamma_{c3}\Delta\omega_2-\gamma_{c2}\Delta\omega_3)}{(\Delta\omega_3-i\gamma_{c3})(\Delta\omega_2-i\gamma_{c2})} \tag{11}$$

where $\Delta\omega_{2,3}=\omega-\omega_{c2,c3}$. The condition for zero transmission can be derived from Eq. (11) as

$$t_{c1}(\Delta\omega_3\Delta\omega_2+\gamma_{c3}\gamma_{c2})=r_{c1}(\gamma_{c2}\Delta\omega_3-\gamma_{c3}\Delta\omega_2) \tag{12}$$

By defining $\theta=\arctan(t_{c1}/r_{c1})$, a set of solutions to Eq. (12) is found as

$$\omega=\omega_{c2}-\gamma_{c2}\tan\frac{\theta}{2}=\omega_{c3}+\gamma_{c3}\tan\frac{\theta}{2} \tag{13}$$

which is referred to as the mode degeneracy condition of Fano resonances. It reduces to $\omega=\omega_{c2}=\omega_{c3}$ in the absence of the straight channel, namely the case of $\theta=0$.

Condition (13) provides the structure optimization guideline to minimize acoustic transmission based on mode degeneracy of Fano resonances. Recall the model of Fig. 2(*f*) with imperfect mode degeneracy. We choose to optimize L_3 to meet the low-transmission condition (13). Acoustic transmission of the improved structure with $L_3=580$ mm is shown in Fig. 2(*f*), and the transmission dip near 874 Hz can be acquired. As a result, the c2-1st and c3-2nd low-T regions can be combined to broaden the sound isolation band. It is worth noting that acoustic resonant transmission at f_{c3}^2 supported by channel c3 locates within the c2-1st low-T region. Therefore, the efficient sound isolation band is eventually constrained in the frequency region between f_{c3}^2 and f_{c3}^4.

To sum up, the mode degeneracy of Fabry–Pérot resonances at $f_{c2}^2=f_{c3}^3$ can lead to zero transmission for systems without the

straight channel. When the straight channel is added, the resonant frequencies are shifted due to Fano resonances, and the mode degeneracy condition for low transmission is changed to Eq. (13). For convenience, when the mode degeneracy at $f_{c2}^2 = f_{c3}^3$ is said in what follows, it refers to the mode degeneracy condition (13) of Fano resonances.

To proceed, we would like to raise a question whether the mode degeneracy at $f_{c2}^2 = f_{c3}^3$ and $f_{c2}^1 = f_{c3}^2$ can be simultaneously achieved. This double-mode degeneracy, if realized, can merge three transmission valleys, namely the c2-1st, c3-1st, and c3-2nd low-T regions, giving rise to a super broad isolation band ranging from f_{c3}^1 to f_{c3}^4. Realization of this double-mode degeneracy is challenging because we always have $f_{c3}^2 = 4f_{c2}^1/3$ if $f_{c2}^2 = f_{c3}^3$ as governed by Eq. (3). The model structure should be improved to meet the degeneracy condition $f_{c3}^2 = f_{c2}^1$ while maintaining $f_{c2}^2 = f_{c3}^3$. In the next section, two strategies will be proposed to conquer this challenge by constructing the direct coupling between channels through micro-hollow holes.

3 Ultra-Broadband Sound Reduction via Double Mode Degeneracy

3.1 Direct Coupling Between Channels c1 and c2. Consider the model that involves channels c1 and c2. It is seen from Fig. 2(*d*) that the dipole resonance of channel c2 at 885 Hz exhibits the anti-symmetric field pattern, and the nodal line with zero pressure lies at the mid-plane, while the monopole resonance at 433 Hz supported by channel c1 is characterized by the symmetric pressure field. Based on these observations, the first strategy we propose is to introduce a micro-hollow hole between two channels, positioned at the mid-plane. Figure 3(*a*) shows the simulation results of acoustic transmission for the model with the hole of width $d_{12} = 0.05$ mm and height 1 mm. It is seen that the presence of the hole can shift the monopole resonance to a higher frequency of 515 Hz. This is due to the fact that adding the hole is equivalent to the reduction of acoustical mass at the location of the aperture, thus making resonance frequencies increase [32]. On the other hand, the micro hole does not impact the dipole resonance at 885 Hz because it locates on the nodal line. Thereby, the mode degeneracy at $f_{c2}^2 = f_{c3}^3$ can be maintained. Figure 3(*b*) shows the simulated acoustic transmission of the three-channel structure having the hole connection. It is found that the mode degeneracy at 885 Hz is preserved, confirming

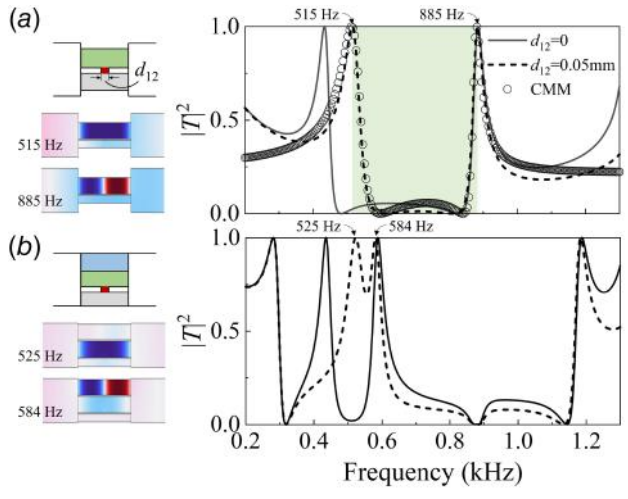

Fig. 3 (*a*) Simulation results of acoustic transmission of two coupled channels c1 and c2 with and without the hole connection, and theoretical results based on the coupled-mode model (CMM) are given for the structure involving the hole connection. (*b*) Simulation results of acoustic transmission of two coupled channels in (*a*) added with the straight pipe.

the weak influence of micro hole on the dipole resonance, while the monopole resonance at 525 Hz supported by channel c2 has been made closer to the dipole resonance 584 Hz of channel c3 in comparison with the unperforated case.

The influence of hole widths d_{12} on Fano resonances can be analyzed based on the coupled-mode model as illustrated in Sec. 2.2. Denote the mode frequency of the monopole (dipole) resonance by ω_- (ω_+), and the corresponding radiation loss by γ_- (γ_+). Let a_- and a_+ represent modal amplitudes of two resonant states with $\mathbf{a} = [a_-, a_+]^{\mathrm{T}}$. Then, the acoustic response of the two-channel structure can still be described by Eq. (4), but the matrices $\mathbf{H}$ and $\mathbf{K}$ are replaced with

$$\mathbf{H} = \begin{bmatrix} \omega_- + i\gamma_- & 0 \\ 0 & \omega_+ + i\gamma_+ \end{bmatrix} \tag{14}$$

and

$$\mathbf{K} = \begin{bmatrix} \sqrt{\gamma_-} & \sqrt{\gamma_+} \\ -\sqrt{\gamma_-} & \sqrt{\gamma_+} \end{bmatrix} \tag{15}$$

Analytic expression of acoustic transmission can be derived from Eq. (7) and then used to determine the coupled-mode parameters $\omega_{+,-}$ and $\gamma_{+,-}$ by fitting the simulation results. The transmission spectrum predicted by the coupled-mode model has been displayed in Fig. 3(*a*), which can capture accurately acoustic responses near resonant states.

Figure 4 shows the coupled-mode parameters for various hole widths. Results show that the mode frequency ω_- of monopole resonance can be enhanced as the aperture width increases. By contrast, the mode frequency ω_+ of dipole resonance remains unchanged against the variation of hole widths because the aperture locates at the nodal line. Besides, the radiation losses of two resonant states show the weak sensitivity to the micro hole. To conclude, the nonlocal effect via the direct coupling between channel c1 and c2 achieved by the hole connection at the mid-plane can shift the monopole resonance towards a higher frequency, while maintaining the dipole resonance frequency unchanged. This provides an efficient strategy to manipulate the double-mode degeneracy.

3.2 Direct Coupling Between Channels c2 and c3. The other route to achieve the double-mode degeneracy employs the hole connection between channel c2 and c3 positioned at the mid-plane. Figure 5(*a*) shows the simulated acoustic transmission of the two-channel structure involving a micro hole of width 0.05 mm and height 1 mm. Channel c3 supports the dipole resonance at frequency 584 Hz, which is unaffected by the hole because it locates at the nodal line as seen by the field distribution. By contrast, the monopole resonance at 442 Hz in channel c2 has been shifted to 505 Hz due to the micro hole effect. On the other hand, two resonant states are degenerate at 882 Hz in the absence of the hole connection. Adding the micro hole does not affect the dipole resonance in channel c2 at this frequency, but has an

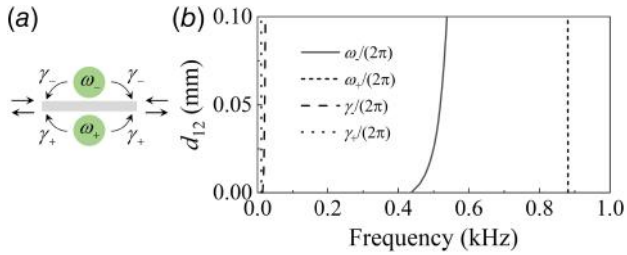

Fig. 4 (*a*) Schematic representation of the coupled-mode model characterizing the resonant state coupling in the two-channel structure involving c1 and c2. (*b*) Mode frequency $\omega_{+,-}$ and radiation loss $\gamma_{+,-}$ for various hole widths.

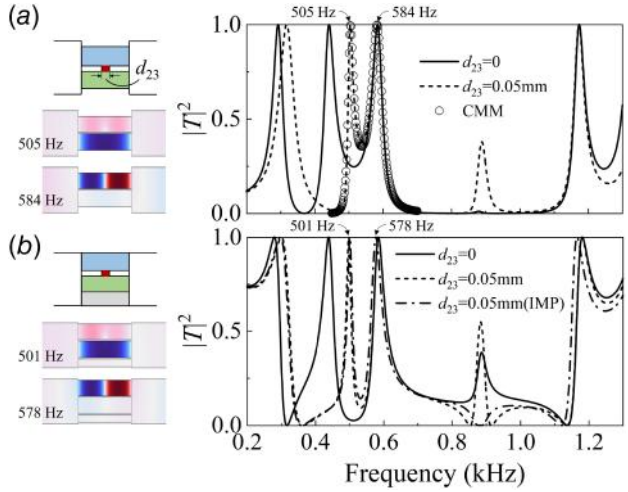

Fig. 5 (*a*) Simulation results of acoustic transmission of two coupled channels c2 and c3 with and without the hole connection, and theoretical results based on the coupled-mode model (CMM) are given for the structure involving the hole connection. (*b*) Simulation results of acoustic transmission of two coupled channels in (*a*) added with the straight pipe, and an additional result for the improved (IMP) structure with $L_3 = 590$ mm is also given.

influence on the monopole resonance frequency in channel c3. Thereby, the degenerate condition at 882 Hz no longer holds, leading to a weak transmission peak near this frequency as seen in Fig. 5(*a*). Although the presence of the micro hole changes both f_{c2}^1 and f_{c3}^3, their shifting magnitudes are different as explained below such that the double-mode degeneracy is still possible.

Figure 5(*b*) shows the acoustic transmission spectrum of three-channel structure with the hole connection between channels c2 and c3. The resonances at 505 Hz and 584 Hz hosted by channels c2 and c3 are slightly modified when the straight pipe is coupled, shifting to 498 Hz and 585 Hz, respectively. In addition, the mode degeneracy at the higher frequency near 882 Hz is still imperfect, accompanied by a transmission enhancement. This mode mismatching can be solved by tuning the channel length L_3, which directly changes resonant frequencies as governed by Eq. (3). Figure 5(*b*) shows by the dash-dotted line the acoustic transmission of the improved structure with $L_3 = 590$ mm, and near-zero transmission near 882 Hz can be gained by this optimization. Notice that this structure modification has a slight influence on low-order resonant frequencies, which are changed to 501 Hz and 578 Hz. The field patterns at these two frequencies confirm that their monopole and dipole resonance properties can be preserved. It can be concluded that the frequency shifting of f_{c2}^1 is larger than f_{c3}^3 by adding the hole connection between channel c2 and c3. Therefore,

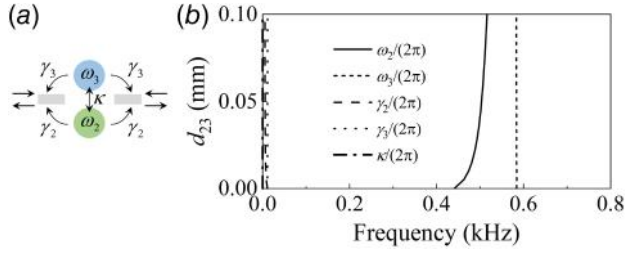

Fig. 6 (*a*) Schematic representation of the coupled-mode model characterizing the resonant state coupling in the two-channel structure involving c2 and c3. (*b*) Mode frequency $\omega_{2,3}$, radiation loss $\gamma_{2,3}$, and coupling magnitude κ for various hole widths.

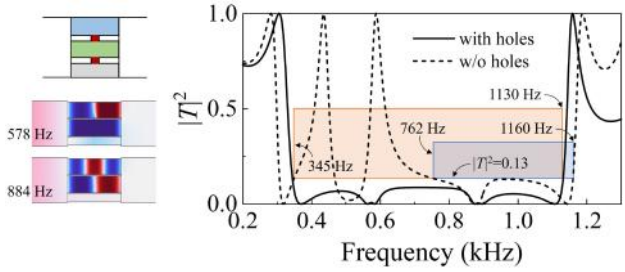

Fig. 7 Simulation results of acoustic transmission of three-channel structures with the hole connection between channels c1 and c2 and that between c2 and c3, and results of Fig. 2(*f*) without the hole connection are replotted here for comparison

an additional mode degeneracy at $f_{c2}^1 = f_{c3}^2$ is possible using this strategy when the degeneracy of high-order modes is preserved.

To disclose the influence of hole apertures d_{23}, the coupled-mode equation (4) is adopted to characterize the coupling interaction of two resonant states at 505 Hz and 584 Hz in Fig. 5(*a*). Denote mode frequencies of these two states by $\omega_{2,3}$, and the corresponding radiation losses by $\gamma_{2,3}$. The coupling magnitude between two states is set as κ, and modal amplitudes are represented by $a_{2,3}$ with $\mathbf{a} = [a_2, a_3]^{\mathrm{T}}$. The matrices $\mathbf{H}$ and $\mathbf{K}$ in Eq. (4) are modified as

$$\mathbf{H} = \begin{bmatrix} \omega_2 + i\gamma_2 & \kappa \\ \kappa & \omega_3 + i\gamma_3 \end{bmatrix} \tag{16}$$

and

$$\mathbf{K} = \begin{bmatrix} \sqrt{\gamma_2} & \sqrt{\gamma_3} \\ -\sqrt{\gamma_2} & \sqrt{\gamma_3} \end{bmatrix} \tag{17}$$

All coupled-mode parameters in $\mathbf{H}$ can be determined by fitting theoretical results of acoustic transmission with simulation ones. The transmission spectrum given by the coupled-mode model has been provided in Fig. 5(*a*), which can well describe acoustic responses of two resonant states near 505 Hz and 584 Hz.

Figure 6 shows the coupled-mode parameters for various hole widths. Although channels c2 and c3 are geometrically connected by the hole, it is interesting to find that the coupling magnitude κ remains vanishingly small for different hole widths. According to Fig. 6, the hole connection functions only for enhancing the monopole resonance frequency of channel c2, and the shifting magnitude increases as the hole aperture is widened. Notice that the resonant frequency f_{c3}^3 will also be affected by the hole, but can be tuned to meet the mode degeneracy condition by optimizing L_3 as suggested in Fig. 5(*b*). Therefore, the hole connection between channels c2 and c3 can provide another effective approach to modulate the double-mode degeneracy.

3.3 Double-Mode Degeneracy Behavior. By adding the hole connection between channels, we have shown that the resonant frequency f_{c2}^1 in channel c2 can be shifted closer to f_{c2}^3 in channel c3, meanwhile the degeneracy of higher-order monopole (f_{c3}^3) and dipole (f_{c2}^2) modes can be maintained. In practical designs, either or both types of hole connections can be adopted depending on the shifting magnitude required. Take the model of Fig. 2(*f*) as an example. Two types of hole connections with $d_{12} = d_{23} = 0.05$ mm are adopted in the following analysis, and the channel length L_3 is optimized as 592 mm to meet the double-mode degeneracy condition. Figure 7 displays the simulated acoustic transmission of the three-channel structure with micro holes, and two transmission dips near 578 Hz and 884 Hz can be clearly seen. From field patterns at 578 Hz, it can be found that the sound reduction arises from the resonant coupling between the 1st-order monopole and 2nd-order dipole modes supported by channels c2 and c3,

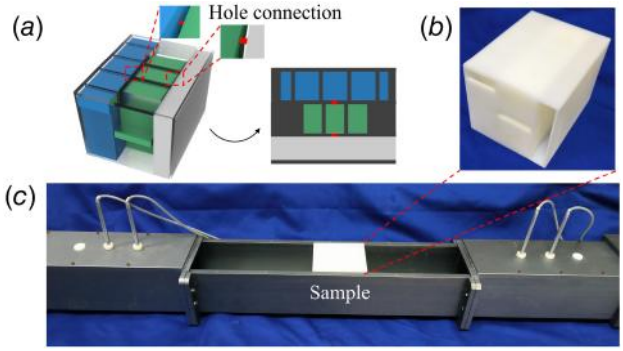

Fig. 8 (*a*) Geometric model and (*b*) sample photograph of the three-channel structure involving the hole connection and (*c*) experiment setup for measuring acoustic scattering coefficients

respectively. The second transmission dip near 884 Hz stems from the coupling between the 2nd-order resonance of channel c2 and the 3rd-order resonance of channel c3 as confirmed by pressure field distribution. According to previous analyses, the nonlocality gained through the hole connection between channels is crucial for achieving this double-mode degeneracy behavior.

Double-mode degeneracy can lead to the ultra-broadband sound isolation. This superior broadband performance can be highlighted by comparison analyses with the unperforated structure of Fig. 2(*f*) as replotted in Fig. 7. The sound isolation band with acoustic transmission lower than $|T|^2 = 0.13$ ranges from 762 Hz to 1160 Hz for the system without adding holes. Define the octave bandwidth as $\mathrm{Log}_2(\mathrm{f_{max}}/\mathrm{f_{min}})$, where $f_{\min}$ and $f_{\max}$ are the lower and upper boundaries of the band, respectively. Then, the octave bandwidth of the unperforated structure is 0.6. Under the same transmission criterion, the octave bandwidth of the perforated structure is up to 1.7 with the frequency band ranging from 345 Hz to 1130 Hz. The octave bandwidth has nearly tripled, demonstrating the superior capability of double-mode degeneracy for a significant increase of the isolation bandwidth.

3.4 Experimental Analyses. Experimental studies are conducted based on the acoustic impedance tube of a square cross section with side length 80 mm, as shown in Fig. 8. The sample is fabricated by 3D printing using Acrylonitrile Butadiene Styrene. The minimum wall thickness of the printed sample is set as 2 mm to ensure acoustic rigidity for airborne sounds. Based on the above experimental environment, a new set of geometric parameters to meet the double-mode degeneracy condition is designed for the three-channel structure: $L_1 = 100$ mm, $L_2 = 388$ mm, $L_3 = 604$ mm, $w_0 = 80$ mm, $w_1 = 76$ mm, $w_2 = 7$ mm, $w_3 = 10$ mm, $h_0 = 80$ mm, $h_1 = 14$ mm, $h_2 = 31$ mm, and $h_3 = 27$ mm. The cylindrical hole of a diameter of 2.1 mm and a height of 2 mm is introduced between channels c1 and c2, while channels c2 and c3 are connected with a hole of a diameter of 2.8 mm and a height of 2 mm. Two holes are both positioned at the mid-plane of coiled channels.

Figures 9(*a*)–9(*c*) show, respectively, simulation results of the sound transmission loss (STL), reflection and absorption in the dampless case. Double-mode degeneracy causes nearly total sound reflection near 587 Hz and 910 Hz as seen in Fig. 9(*b*), giving rise to the broadband sound isolation as similar to the behavior disclosed in Fig. 7. In practical situations, acoustic damping is usually inevitable. To analyze the impact of acoustic damping, the Narrow Region Acoustics module is adopted in COMSOL MULTIPHYSICS to simulate the viscous thermal losses within channels, and the results are shown in Fig. 9. It is seen from Fig. 9(*c*) that the degenerate resonant modes can significantly enhance acoustic absorption near 587 Hz and 910 Hz. In this case, the high STL is still obtained due to strong acoustic damping, although sound reflection is weakened. As a result, the broadband isolation behavior can also be achieved in the damped case due to the joint action of high sound absorption and reflection. The measured results of the STL, reflection, and absorption spectra have been displayed in Fig. 9, confirming the prediction of numerical simulation involving acoustic damping. The experimental STL exceeds 7 dB in the frequency range of 300–1133 Hz with the octave bandwidth up to 1917. The sample thickness is 1/4.79 of the wavelength of the band center frequency, and the area ratio between the straight channel and waveguide, which characterizes the air ventilation rate, is 16.6%. Experimental results clearly demonstrate the ultra-broadband sound reduction caused by double-mode degeneracy.

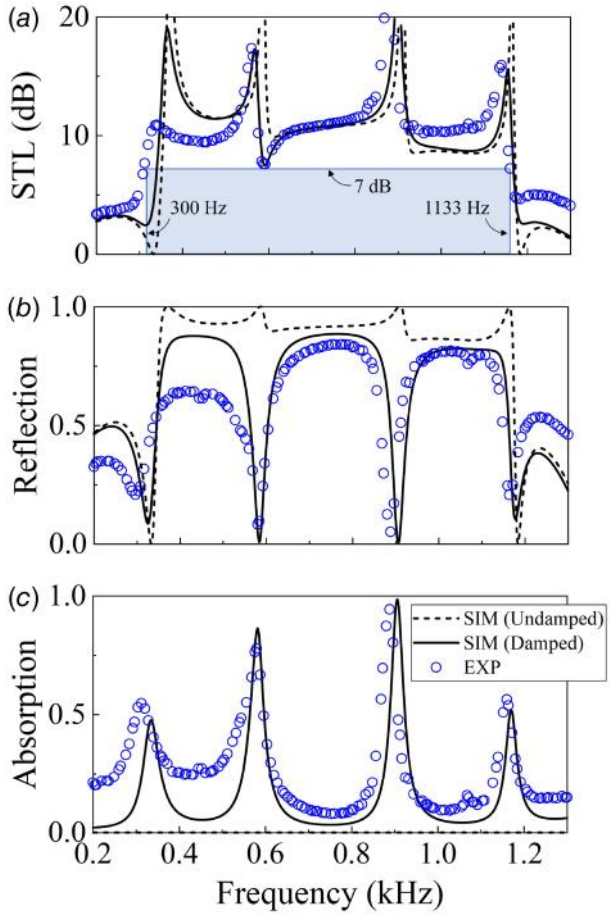

Fig. 9 Experimental results of (*a*) the STL, (*b*) reflection, and (*c*) absorption coefficients of the three-channel structure with double-mode degeneracy, as well as simulation results with and without incorparating acoustic damping

4 Conclusion

In a ternary coiling-channel structure, a novel mechanism for broadband sound isolation is proposed by using the nonlocal effect via direct mode couplings. The coupled-mode theory is adopted to derive the mode degeneracy condition of Fano resonances. Based on this condition, two transmission valleys that are independently tuned by two coiling channels can be combined to broaden the isolation bandwidth. Three transmission valleys can be merged if an additional mode degeneracy can be created, which, however, is impossible to achieve because of the inherent limitation of integer resonances. Our idea to conquer this challenge is to introduce the direct coupling between channels, which can shift specific resonant frequencies closer to a new degenerate

state while preserving the mode degeneracy already existed. In a proof-of-concept model, simulation results show that the octave bandwidth of sound isolation can nearly triple when the direct coupling is added, clearly demonstrating its superior performance for enhancing the bandwidth. Finally, ventilating structures with double-mode degeneracy are designed and fabricated. Experimental measurements are conducted to validate the ultra-broadband sound isolation arising from double-mode degeneracy.

Acknowledgment

This work was supported by the National Natural Science Foundation of China (12225203, 11622215, 11872111, 11991030, and 11991033) and 111 Project (B16003).

Conflict of Interest

There are no conflicts of interest.

Data Availability Statement

The datasets generated and supporting the findings of this article are obtainable from the corresponding author upon reasonable request.

References

[1] Zhen, N., Huang, R.-R., Fan, S.-W., Wang, Y.-F., and Wang, Y.-S., 2025, "Resonance-Based Acoustic Ventilated Metamaterials for Sound Insulation," npj Acoustics, **1**(1), pp. 1–23.
[2] Long, H., Liu, C., Shao, C., Cheng, Y., Tao, J., Qiu, X., and Liu, X., 2020, "Tunable and Broadband Asymmetric Sound Absorptions With Coupling of Acoustic Bright and Dark Modes," J. Sound Vib., **479**, p. 115371.
[3] Meng, Y., Romero-García, V., Gabard, G., Groby, J., Bricault, C., and Goudé, S., 2023, "Subwavelength Broadband Perfect Absorption for Unidimensional Open-Duct Problems," Adv. Mater. Technol., **8**(12), p. 2201909.
[4] Crivoi, A., Du, L., and Fan, Z., 2023, "Ventilated Acoustic Meta-Barrier Based on Layered Helmholtz Resonators," Appl Acoust., **205**, p. 109263.
[5] Jiménez, N., Romero-García, V., Pagneux, V., and Groby, J.-P., 2017, "Quasiperfect Absorption by Subwavelength Acoustic Panels in Transmission Using Accumulation of Resonances Due to Slow Sound," Phys. Rev. B, **95**(1), p. 014205.
[6] Lee, T., Nomura, T., Dede, E. M., and Iizuka, H., 2020, "Asymmetric Loss-Induced Perfect Sound Absorption in Duct Silencers," Appl. Phys. Lett., **116**(21), p. 214101.
[7] Gao, C., Hu, C., Hou, B., Zhang, X., Li, S., and Wen, W., 2023, "Ventilation Duct Silencer Design for Broad Low-Frequency Sound Absorption," Appl Acoust., **206**, p. 109324.
[8] Fu, C., Zhang, X., Yang, M., Xiao, S., and Yang, Z., 2017, "Hybrid Membrane Resonators for Multiple Frequency Asymmetric Absorption and Reflection in Large Waveguide," Appl. Phys. Lett., **110**(2), p. 021901.
[9] Wang, S., Tao, J., Qiu, X., and Burnett, I. S., 2022, "A Natural Ventilation Window for Transformer Noise Control Based on Coiled-Up Silencers Consisting of Coupled Tubes," Appl Acoust., **192**, p. 108744.
[10] Nguyen, H., Wu, Q., Xu, X., Chen, H., Tracy, S., and Huang, G., 2020, "Broadband Acoustic Silencer With Ventilation Based on Slit-Type Helmholtz Resonators," Appl. Phys. Lett., **117**(13), p. 134103.
[11] Kumar, S., Xiang, T. B., and Lee, H. P., 2020, "Ventilated Acoustic Metamaterial Window Panels for Simultaneous Noise Shielding and Air Circulation," Appl Acoust., **159**, p. 107088.
[12] Ye, Y., Wu, C., Kang, S., Gao, C., Yan, Z., Huang, Y., and Wu, X., 2023, "Reconfigurable Ultra-Sparse Ventilated Metamaterial Absorber," APL Mater., **11**(12), p. 121117.
[13] Qi, H.-B., Fan, S.-W., Jiang, M., Tang, X.-L., and Wang, Y.-S., 2024, "Low-Frequency Ultra-Broadband Ventilated Muffler Based on a Resonance-Labyrinthine Metamaterial," Extreme Mech. Lett., **67**, p. 102120.
[14] Chen, A., Zhao, X., Yang, Z., Anderson, S., and Zhang, X., 2022, "Broadband Labyrinthine Acoustic Insulator," Phys. Rev. Appl., **18**(6), p. 64057.
[15] Li, X., Zhang, H., Tian, H., Huang, Y., and Wang, L., 2022, "Frequency-Tunable Sound Insulation via A Reconfigurable and Ventilated Acoustic Metamaterial," J Phys. D: Appl. Phys., **55**(49), p. 495108.
[16] Yang, J., Lee, J. S., Lee, H. R., Kang, Y. J., and Kim, Y. Y., 2018, "Slow-Wave Metamaterial Open Panels for Efficient Reduction of Low-Frequency Sound Transmission," Appl. Phys. Lett., **112**(9), p. 091901.
[17] Kumar, S., and Lee, H. P., 2020, "Labyrinthine Acoustic Metastructures Enabling Broadband Sound Absorption and Ventilation," Appl. Phys. Lett., **116**(13), p. 134103
[18] Zhang, R., Wang, G., Zhou, X., and Hu, G., 2022, "A Decoupling-Design Strategy for High Sound Absorption in Subwavelength Structures With Air Ventilation," JASA Express. Lett., **2**(3), p. 033602.
[19] Ghaffarivardavagh, R., Nikolajczyk, J., Anderson, S., and Zhang, X., 2019, "Ultra-Open Acoustic Metamaterial Silencer Based on Fano-Like Interference," Phys. Rev. B, **99**(2), p. 024302.
[20] Zhang, R., Zhang, L., Hu, G., and Zhou, X., 2025, "Sound Mitigation by Metamaterials With Low-Transmission Flat Band," ASME J. Appl. Mech., **92**(1), p. 011009.
[21] Xiao, Z., Gao, P., Wang, D., He, X., and Wu, L., 2021, "Ventilated Metamaterials for Broadband Sound Insulation and Tunable Transmission at Low Frequency," Extreme Mech. Lett., **46**, p. 101348.
[22] Su, Z., Zhu, Y., Gao, S., Luo, H., and Zhang, H., 2022, "High-Efficient and Broadband Acoustic Insulation in A Ventilated Channel With Acoustic Metamaterials," Front. Mech. Eng., **8**, p. 857788.
[23] Chen, J.-S., Chung, Y.-T., Wang, C.-Y., Lo, W.-Y., Liu, C.-H., Yu, C.-H., Chang, I.-L., and Lin, T.-R., 2023, "Ultrathin Arch-Like Labyrinthine Acoustic Metasurface ForLow-Frequency Sound Absorption," Appl Acoust., **202**, p. 109142.
[24] Nguyen, H., Wu, Q., Chen, H., Chen, J., Yu, Y., Tracy, S., and Huang, G., 2021, "A Fano-Based Acoustic Metamaterial for Ultra-Broadband Sound Barriers," Proc. R. Soc. A, **477**(2248), p. 20210024.
[25] Xiang, L., Wang, G., Zhu, C., Shi, M., Hu, J., and Luo, G., 2022, "Ventilation Barrier With Space-Coiling Channels of Varying Cross-Section for Broadband Sound Insulation," Appl Acoust., **201**, p. 109110.
[26] Sun, M., Fang, X., Mao, D., Wang, X., and Li, Y., 2020, "Broadband Acoustic Ventilation Barriers," Phys. Rev. Appl., **13**(4), p. 044028.
[27] Lin, D.-K., Xiao, X.-W., Yang, C.-C., Ho, S.-Y., Chou, L.-C., Chiang, C.-H., Chen, J.-S., and Liu, C.-H., 2024, "An Acoustic Impedance Design Method for Tubular Structures With Broadband Sound Insulations and Efficient Air Ventilation," Appl Acoust., **220**, p. 109983.
[28] Tang, Y., Liang, B., and Lin, S., 2022, "Broadband Ventilated Meta-Barrier Based on the Synergy of Mode Superposition and Consecutive Fano Resonances," J. Acoust. Soc. Am., **152**(4), pp. 2412–2418.
[29] Zhu, Y., Dong, R., Mao, D., Wang, X., and Li, Y., 2023, "Nonlocal Ventilating Metasurfaces," Phys. Rev. Appl., **19**(1), p. 014067.
[30] Zhang, Y., Zhang, L., Duan, Y., and Zhou, X., 2025, "Broadband Sound Reduction in Space-Coiling Ventilation Structures With Microperforated Shells," Appl Acoust., **235**, p. 110676.
[31] Ji, J., Li, J., Cummer, S. A., and Jing, Y., 2023, "Ultra-Sparse Near-Perfect Sound Absorbers," JASA Express Lett, **3**(3), p. 034001.
[32] Xiaopai, Z., Xiaojun, Q., and Jie, P., 2012, "Effect of an Aperture on Enclosure Resonance Characteristics," Acta Acust., **37**(4), pp. 353–362.